Supporting Information for 'Linking Intra-Plate Volcanism to Lithospheric Structure and Asthenospheric Flow'

DOI: 10.1002/2021GC009953

Thomas Duvernay[1], D. Rhodri Davies[1], Christopher R. Mathews[1], Angus H. Gibson[1], Stephan C. Kramer[2]

[1]Research School of Earth Sciences, The Australian National University, Canberra, ACT, Australia

[2]Department of Earth Science and Engineering, Imperial College London, London, UK

Contents of this file

Corresponding author: Thomas Duvernay, Research School of Earth Sciences, The Australian National University, 142 Mills Rd, Acton ACT 0200, Australia. (thomas.duvernay@anu.edu.au)

Melting Parameterisation

McKenzie (1984) defined a framework to calculate the amount of melt produced through decompression at constant entropy. Writing the total differential of entropy as a function of temperature, pressure and melt fraction, the following two governing equations are obtained:

$$\left.\frac{dF}{dP}\right|_S = \frac{-\frac{c_P}{T}\left.\frac{dT}{dP}\right|_F + \frac{\alpha_s}{\rho_s} + F\left(\frac{\alpha_f}{\rho_f} - \frac{\alpha_s}{\rho_s}\right)}{\Delta S + \frac{c_P}{T}\left.\frac{dT}{dF}\right|_P}, \tag{1}$$

$$\left.\frac{dT}{dP}\right|_S = \frac{\frac{\alpha_s}{\rho_s} + F\left(\frac{\alpha_f}{\rho_f} - \frac{\alpha_s}{\rho_s}\right) - \Delta S\left.\frac{dF}{dP}\right|_S}{\frac{c_P}{T}}. \tag{2}$$

In the above expressions, P, T and F represent the pressure, temperature and fraction of melt, respectively. The coefficient of thermal expansion, density and the specific heat at constant pressure are denoted by α, ρ and c_P, while S corresponds to entropy and ΔS to the entropy of fusion. Subscripts s and f differentiate between the solid and fluid phase, respectively, while derivative sub-scripts indicate variables that are held constant.

In the absence of melting, Equations 1 and 2 become:

$$\left.\frac{dF}{dP}\right|_S = 0, \tag{3}$$

$$\left.\frac{dT}{dP}\right|_S = \frac{\alpha_s T}{\rho_s c_P}. \tag{4}$$

In particular, Equation 4 represents the temperature change of a parcel of rock ascending adiabatically through Earth's mantle. However, in our numerical models, we can already calculate a temperature change as we are solving the heat equation for temperature. To ensure consistency between the evolution of temperature obtained through the melting

framework and the thermal state of our model, we modify the framework's governing equations: we replace the adiabatic gradient term by the actual temperature gradient derived from the temperature field calculated by Fluidity. Mathematically, using thermodynamical identities, our modification translates to

$$\frac{\alpha}{\rho} = -\frac{dS}{dP}\bigg|_T = \frac{dS}{dT}\bigg|_P \frac{dT}{dP}\bigg|_S \sim \frac{c_P}{T}\frac{dT}{dP}\bigg|^{Fluidity},$$

and, in the absence of melting, it leads to

$$\frac{dT}{dP}\bigg|_S \sim \frac{dT}{dP}\bigg|^{Fluidity}.$$

Incorporating this change within Equations 1 and 2, we obtain the following system of coupled equations:

$$\frac{dF}{dP}\bigg|_S = \frac{\dfrac{dT}{dP}\bigg|^{Fluidity} - \dfrac{dT}{dP}\bigg|_F^{Katz}}{\dfrac{T\Delta S}{c_P} + \dfrac{dT}{dF}\bigg|_P^{Katz}} \tag{5}$$

$$\frac{dT}{dP}\bigg|_S = \frac{dT}{dP}\bigg|^{Fluidity} - \frac{T\Delta S}{c_P}\frac{dF}{dP}\bigg|_S. \tag{6}$$

In the above expressions, derivative super-scripts signal where the expression/value for the derivative is sourced from.

References

McKenzie, D. (1984). The generation and compaction of partially molten rock. *Journal of Petrology*, *25*(3), 713–765.

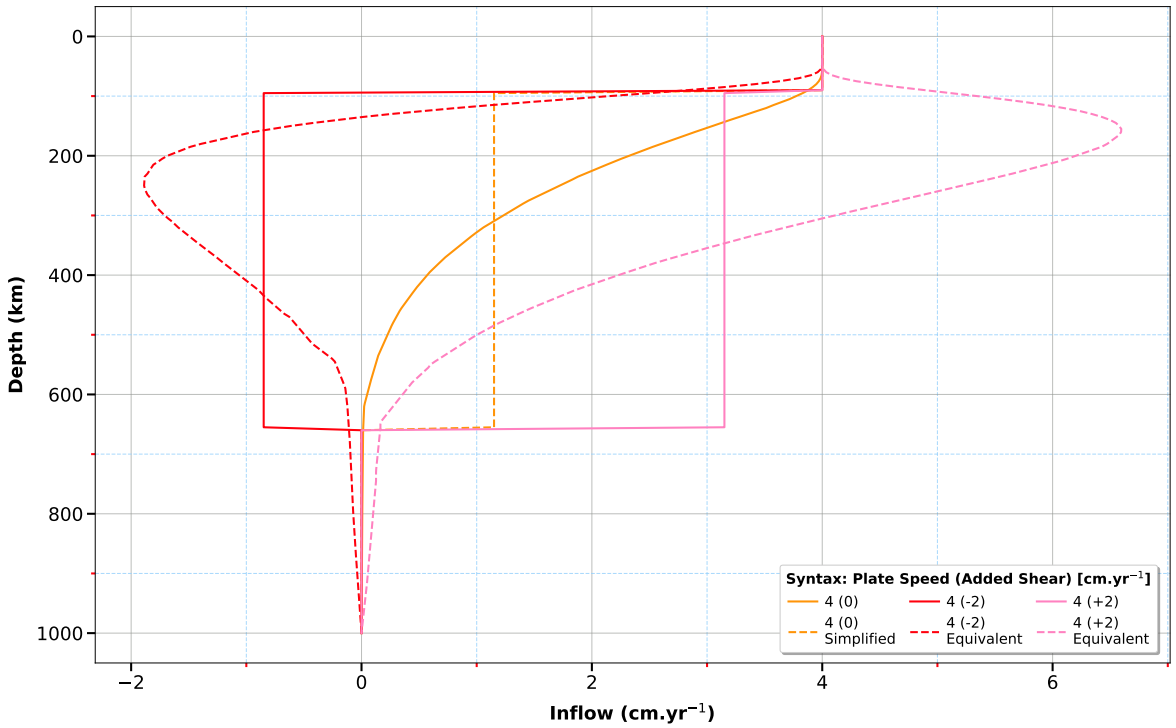

Figure S1. Velocity inflow profiles considered in the study (solid lines) and their counterparts used to demonstrate equivalent flow patterns (dashed lines). The '4 (0)' profile is measured within the oceanic realm of the purely plate-driven model. The '4 (0) Simplified' profile corresponds to a step-like version of the '4 (0)' profile, with plate velocity imposed from the surface down to 90 km (our initial LAB), constant velocity imposed within the asthenosphere (where the integral of velocity is identical to the '4 (0)' profile over this depth range), and zero flow imposed in the lower mantle. Profiles '4 (-2)' and '4 (+2)' build on the '4 (0) Simplified' profile by adding 2 cm yr^{-1} asthenospheric shear, either aligned with (+2) or opposite to (-2) plate motion. Profiles '4 (-2) Equivalent' and '4 (+2) Equivalent' are measured within the oceanic realm, from simulations where the '4 (-2)' and '4 (+2)' profiles are imposed at the inflow boundary.

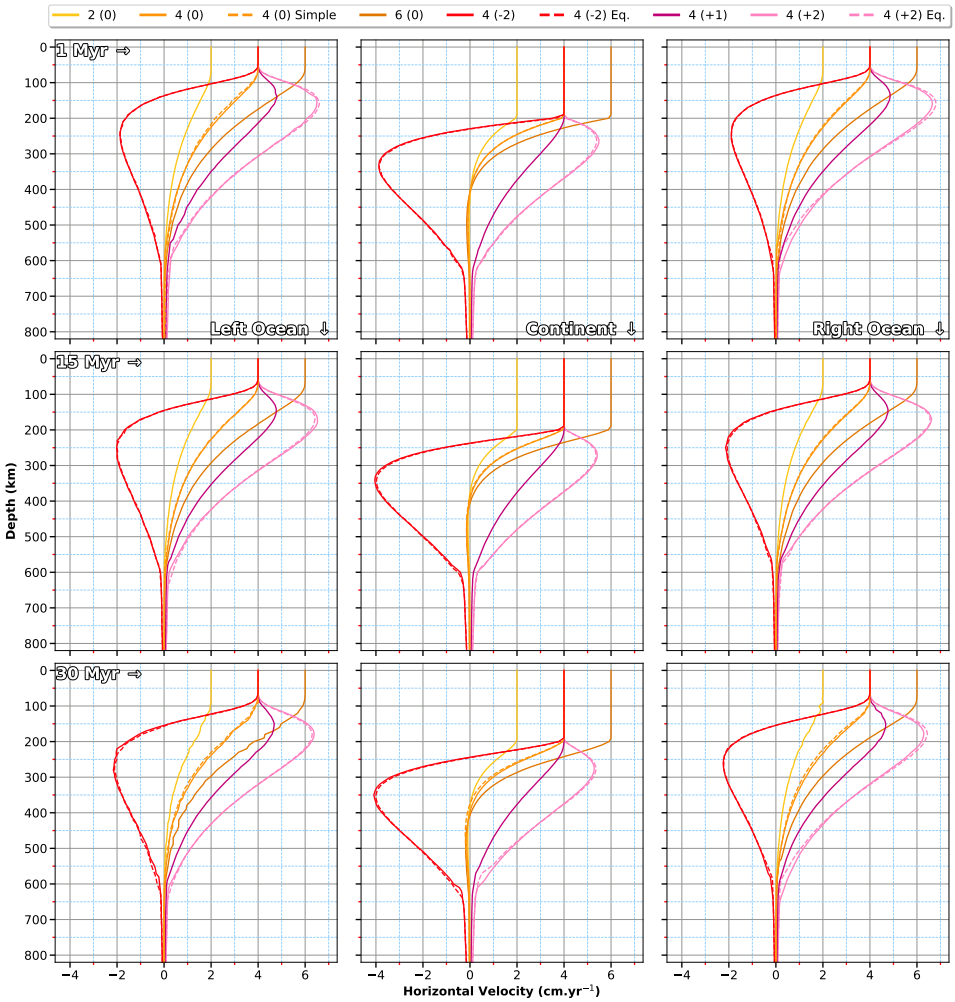

Figure S2. Velocity profiles generated within the numerical domain when plate motion and, in some cases, additional asthenospheric shear, are prescribed. Specifically, the profiles displayed in Figure S1 are prescribed as inflow boundary conditions for different models, in addition to cases with increased ('6 (0)') or decreased ('2 (0)') plate velocities. The resulting flow field is sampled below oceanic lithosphere to the left of the continent (left), below the continent (centre) and below oceanic lithosphere to the right of the continent (right). Additionally, different rows display profiles measured at 1 Myr, 15 Myr and 30 Myr, respectively. We find that cases where simplified step-function profiles are imposed at the inflow boundary yield results that are practically indistinguishable from the smoother profiles. This demonstrates that results are largely insensitive to the depth-dependence of the inflow profile prescribed within the asthenosphere – the flow is redistributed in line with the underlying physics.

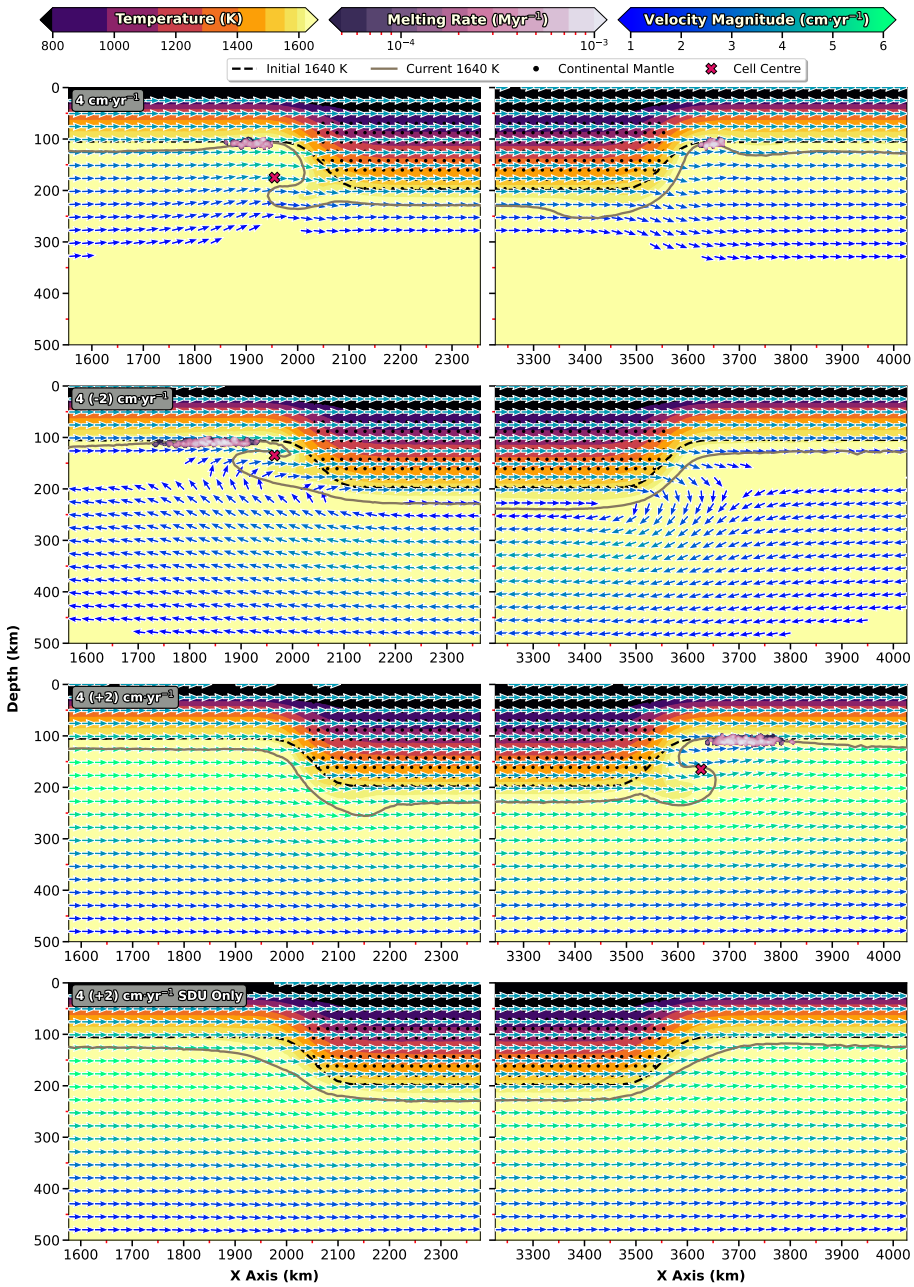

Figure S3. Effect of plate motion and asthenospheric flow on dynamics adjacent to lithospheric steps. The top row illustrates our $4\,\mathrm{cm\,yr^{-1}}$ purely plate-driven scenario, while the subsequent two rows display results following the addition of momentum within the asthenosphere, opposite to and aligned with plate motion, respectively. The bottom row is equivalent to the third row, except that the coefficient of thermal expansion has been set to 0; all models are displayed after 20 Myr. Graphic illustration similar to Figure 4, with glyphs only drawn where velocities exceed $1\,\mathrm{cm\,yr^{-1}}$; the velocity field is that directly output from the model.

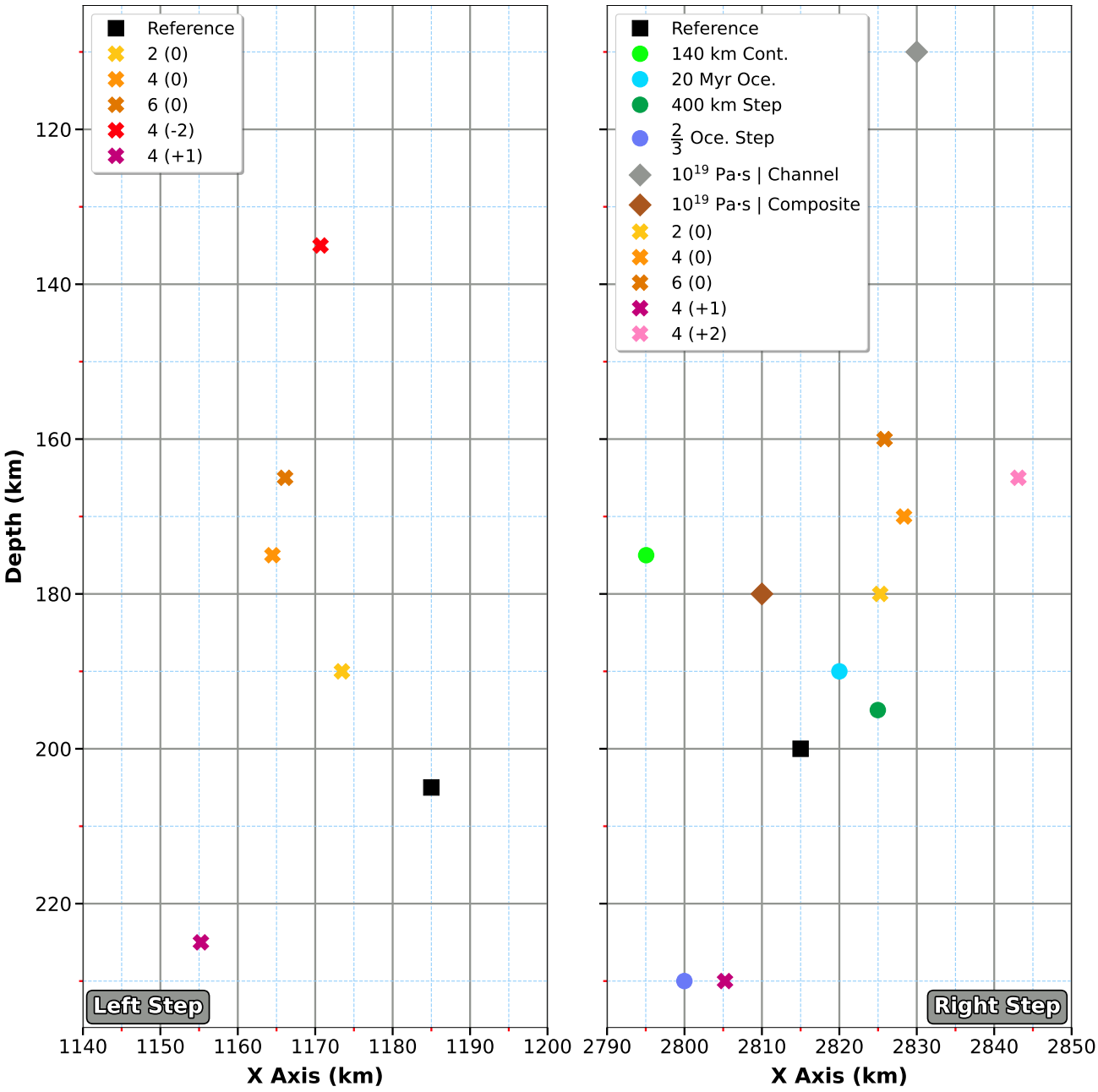

Figure S4. Location of cell centres used as a basis for vertical velocity profiles in Figure 5, determined at the time of maximum downwelling velocity as illustrated in Figure S5. Cases with plate motion are corrected for plate advection through time.

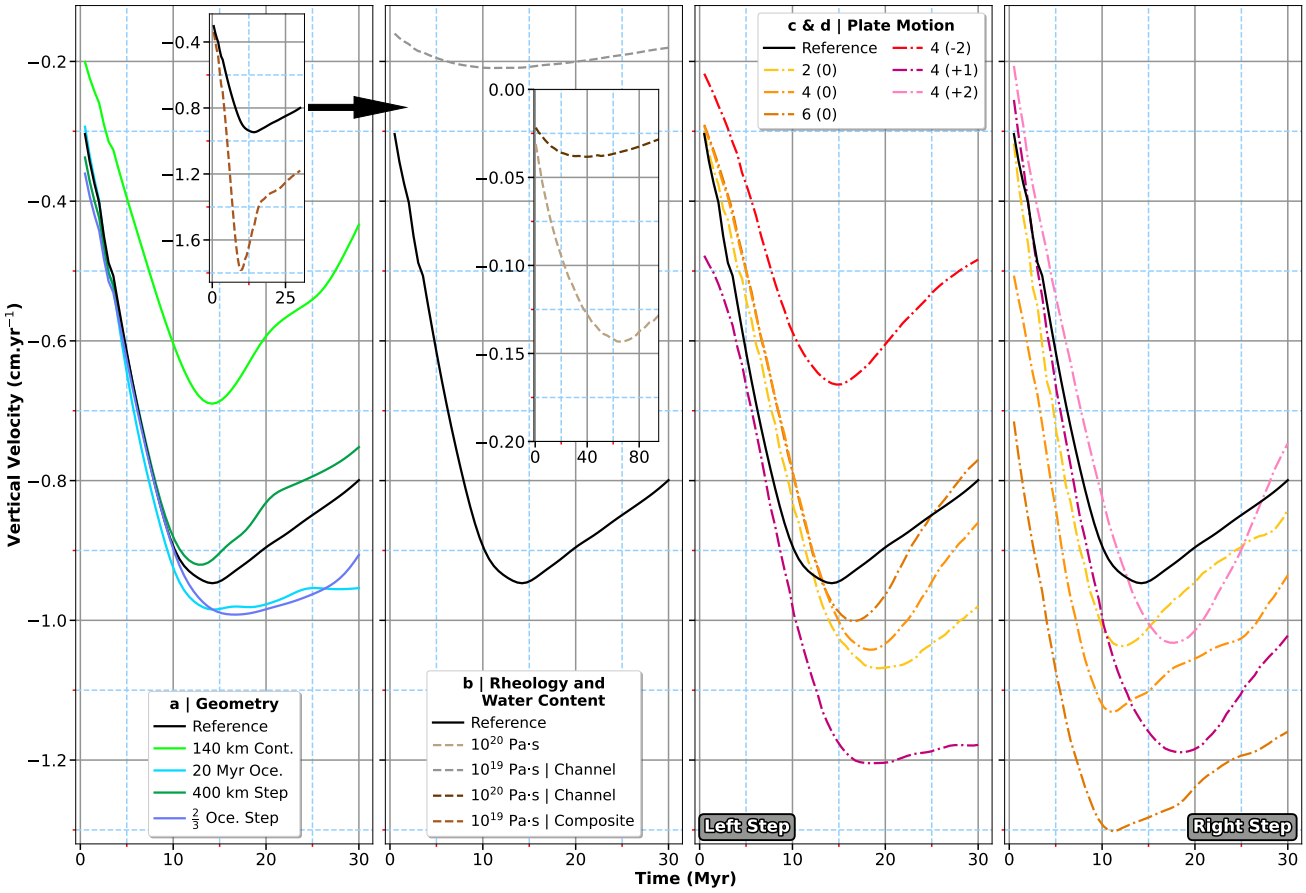

Figure S5. Maximum downwelling velocity, as a function of time, at the right step (if not specified). The velocity field is analysed over an area surrounding the step, no deeper than continental depth. Each curve has a local minimum, which we use to determine the time at which we compare the vigour of edge-driven instabilities cases across our chosen parameter space (Figure 5). Such a strategy allows for a meaningful comparison between different cases. (a) Effect of step geometry. The inset compares the reference case to the composite rheology model and, therefore, belongs with the cases shown on panel b as indicated by the black arrow. (b) Role of viscosity. The inset corresponds to a zoom on the 10^{20} Pa s cases, with a similar aspect ratio as the original panel. (c) & (d) Influence of plate motion and asthenospheric shear.

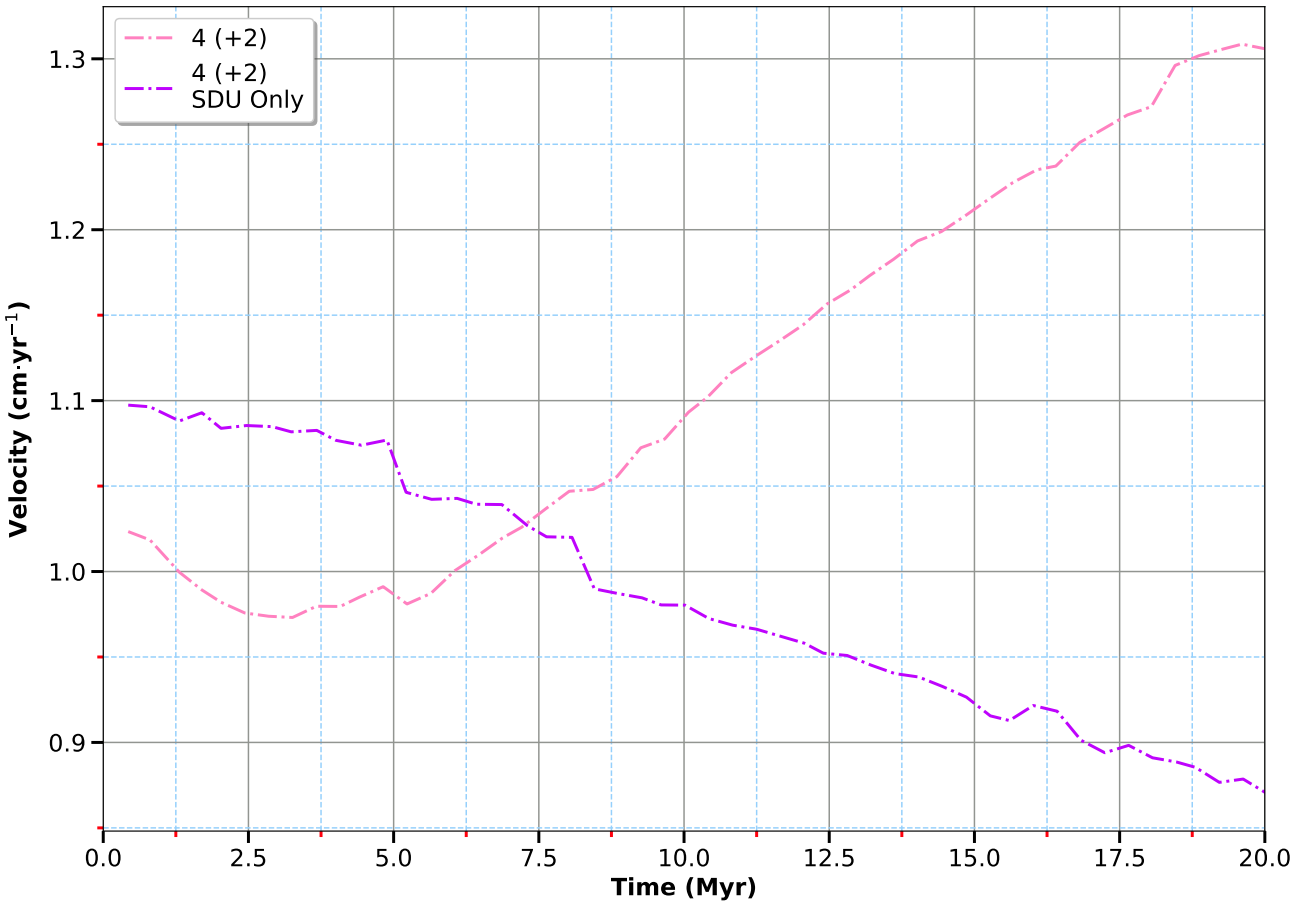

Figure S6. Temporal evolution of the maximum upwelling velocity recorded at the right step for cases with additional asthenospheric shear of $2\,\mathrm{cm\,yr^{-1}}$ prescribed at the inflow boundary. Case '4 (+2)' incorporates both EDC and SDU mechanisms, while case '4 (+2) SDU Only' solely features SDU (the coefficient of thermal expansion is set to 0).

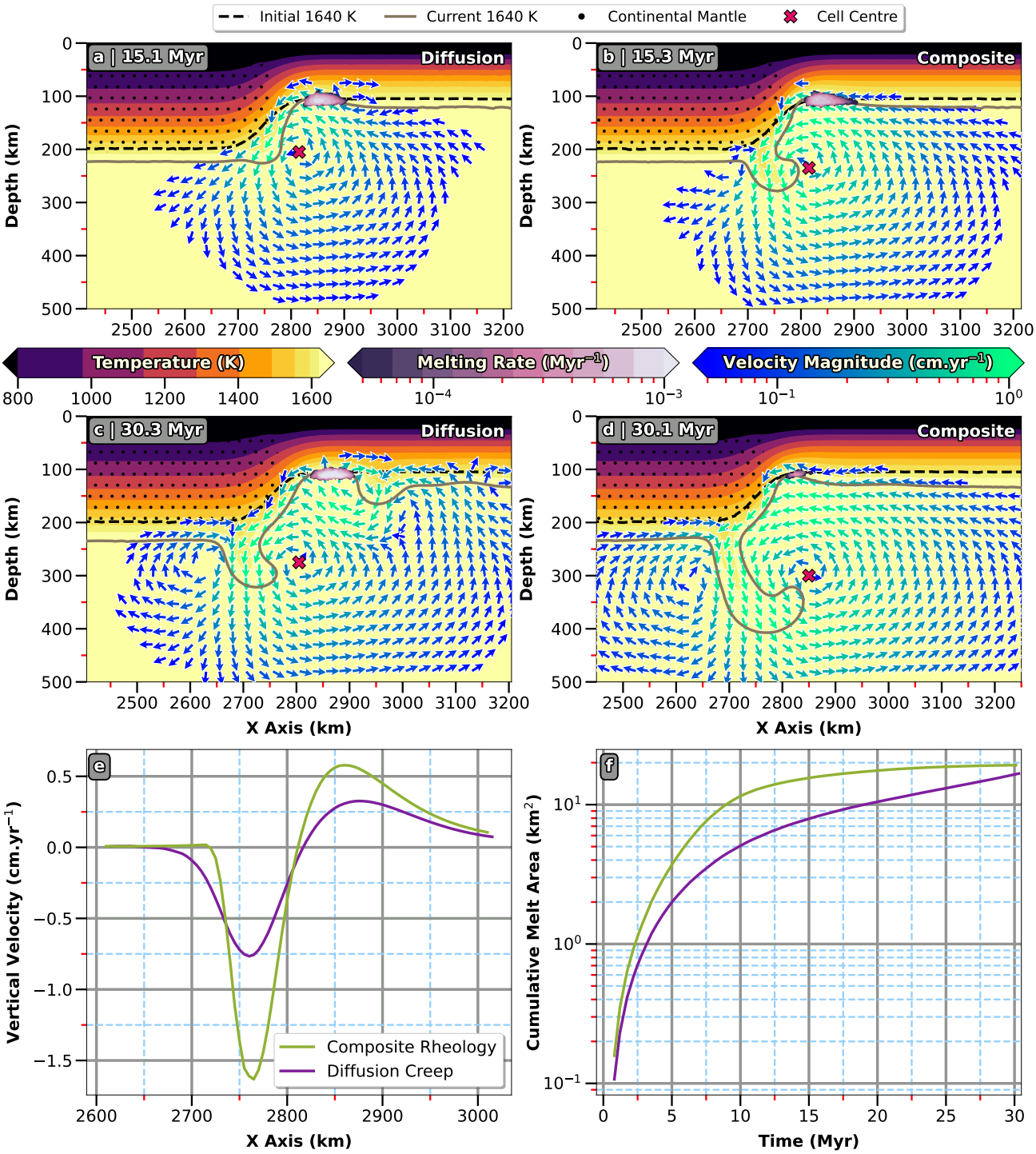

Figure S7. Dynamics (a-e) and melt production (f) compared between the reference case (a & c) and the model incorporating a composite rheology (b & d).

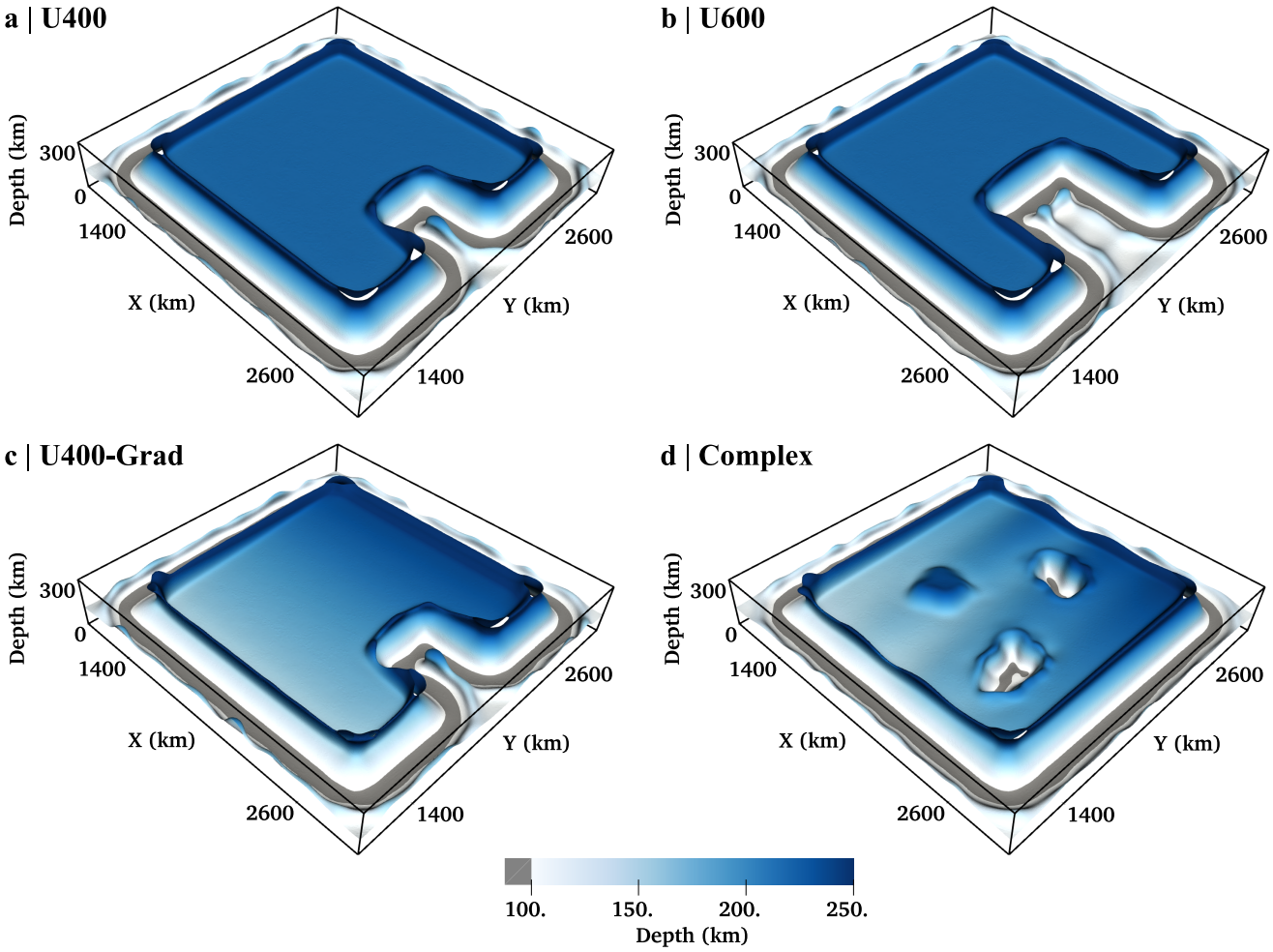

Figure S8. Topography at the LAB, as delineated by the 1620 K isotherm, for continental geometries used in 3-D simulations. Cases are illustrated after 30 Myr of model evolution. (a) Case U400. (b) Case U600. (c) Case U400-Grad. (d) Case Complex.

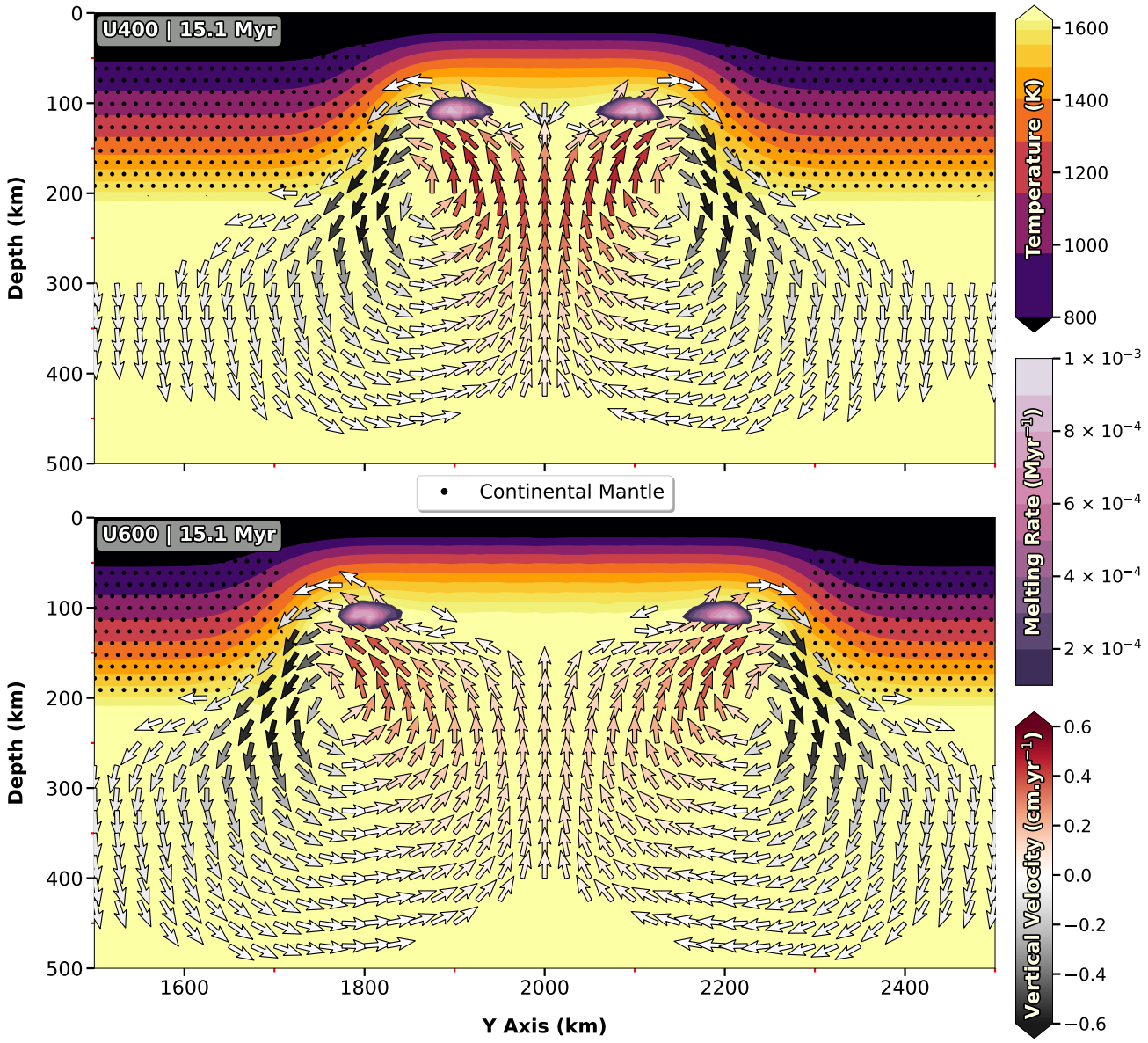

Figure S9. Influence of the indent's width on the flow dynamics, as observed after 15 Myr. Background colours represent temperature. Black dots depict the location of continental mantle. Arrow glyphs illustrate the velocity field and their colour indicates the strength of flow. Areas experiencing melting are represented as a superimposed surface, coloured by melting rate.

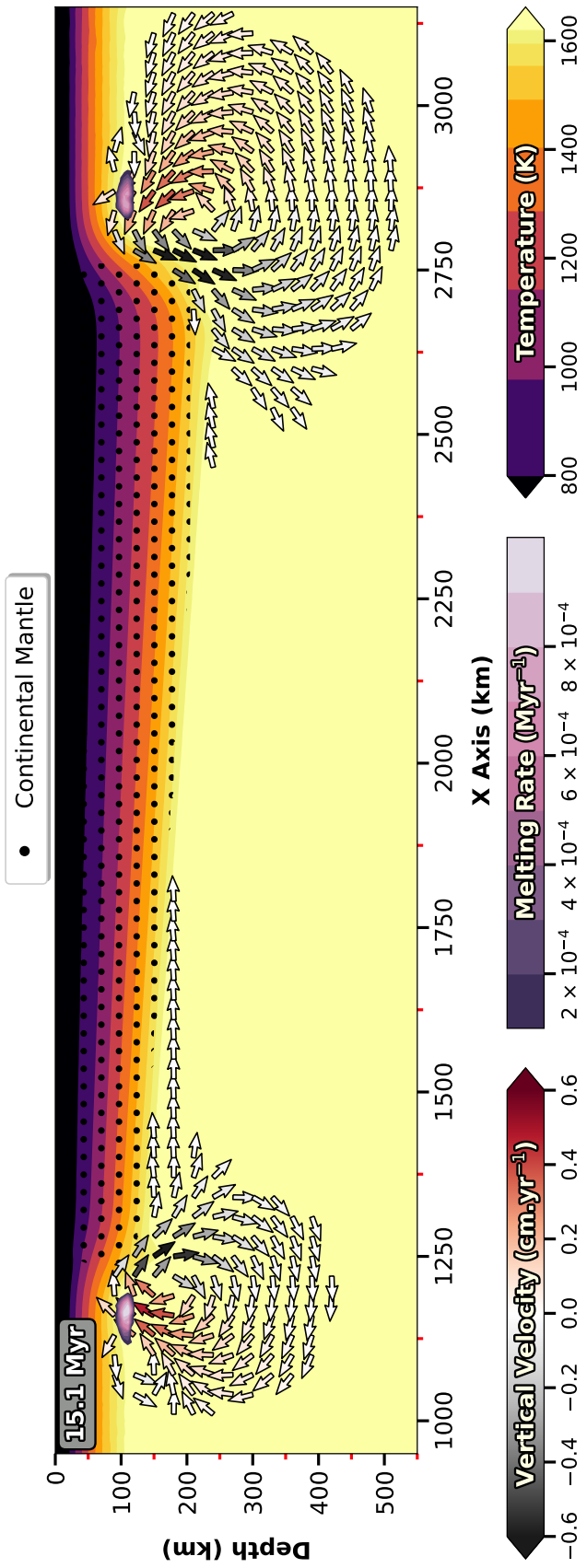

Figure S10. Effect of continental thickness on edge-driven cell development, as observed after 15 Myr for Case U400-Grad. Background colours represent temperature. Black dots depict the location of continental mantle. Arrow glyphs illustrate the velocity field and their colour indicates the strength of the flow. Particles that record active melting are represented by a superimposed surface, coloured by melting rate.

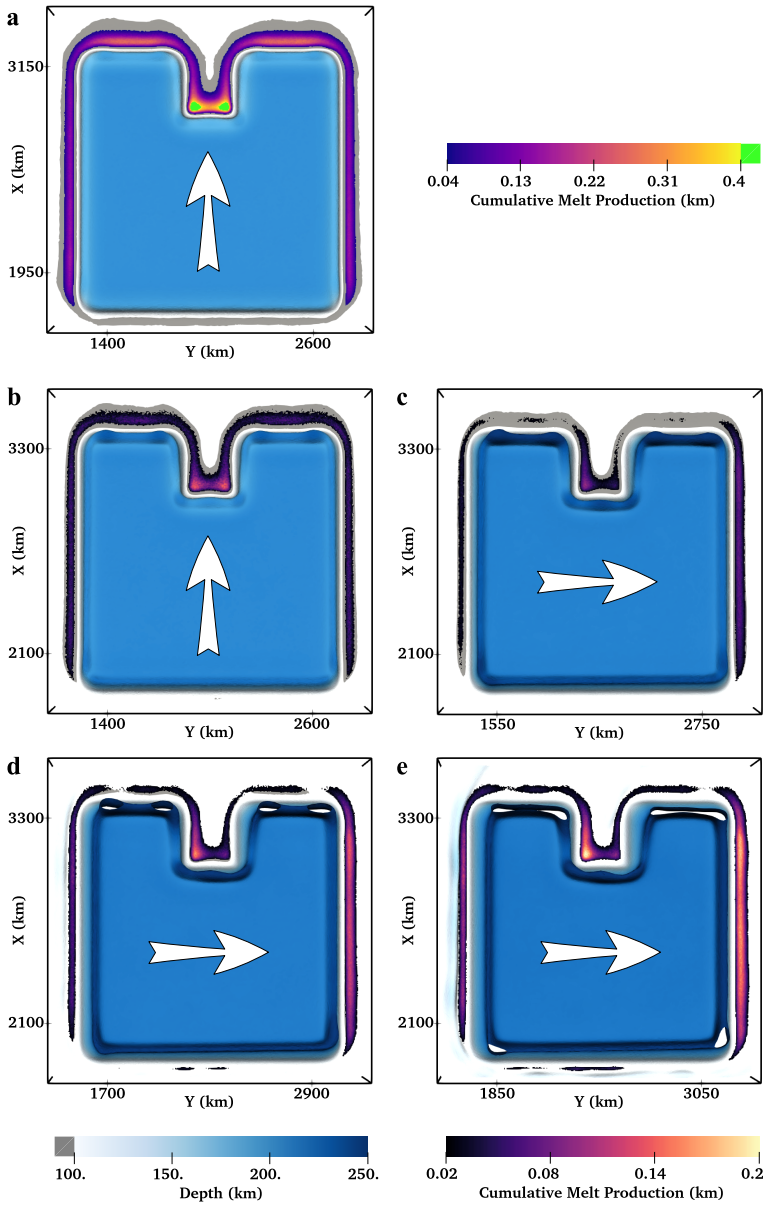

Figure S11. Melt production around the continent following a 90° change in prescribed plate motion and inflow direction at 16 Myr for the positive-x model. Large white arrows represent both the direction of plate motion and the direction of asthenospheric flow relative to the continent, and point from the continent's leading edge to its trailing edge. (a) Cumulative melt production after 12 Myr. (b) Cumulative melt production between 12 Myr and 16 Myr. (c) Cumulative melt production between 16 Myr and 20 Myr (i.e. immediately following the change in imposed flow direction). (d) Cumulative melt production between 16 Myr and 24 Myr. (e) Cumulative melt production between 16 Myr and 28 Myr.

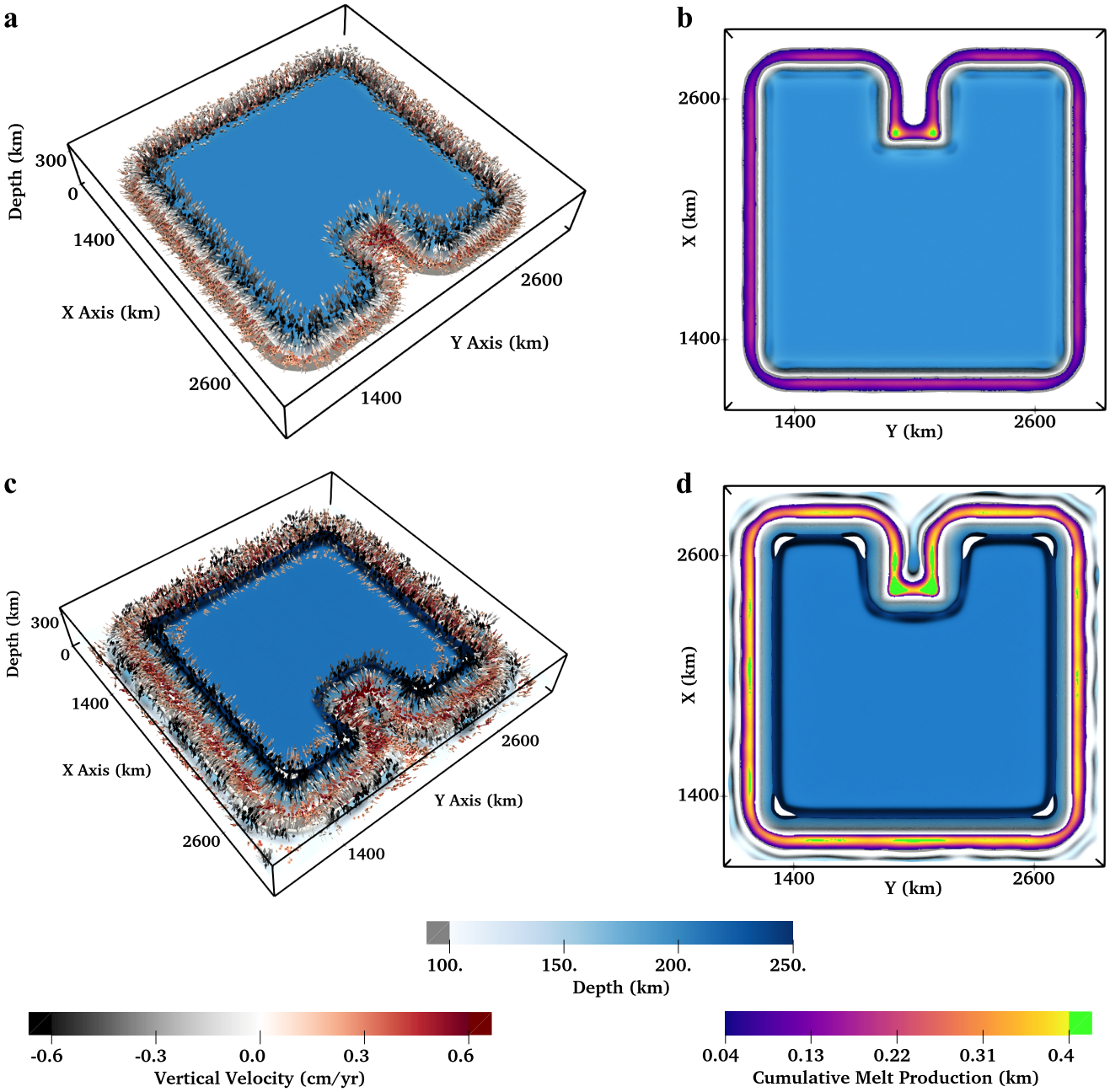

Figure S12. Comparison of the flow dynamics and melt production adjacent to the continent over time for Case U400. Graphic illustration is similar to Figures 7 and 8. (a) Velocity field after 15 Myr. (b) Cumulative melt production after 15 Myr. (c) Velocity field after 30 Myr. (d) Cumulative melt production after 30 Myr.